Harnessing Satellite Constellations as Signals of Opportunity for Atmospheric Forecasting and Enhanced Space Situational Awareness

David J. Fitzpatrick*
Ann and H.J. Smead Department of Aerospace Engineering Sciences, University of Colorado Boulder

Eric K. Sutton†
Space Weather Technology, Research, and Education Center (SWx TREC), University of Colorado Boulder

Marcin Pilinski‡
Laboratory for Atmospheric and Space Physics, University of Colorado Boulder

ABSTRACT

Enhancing the accuracy of Low-Earth Orbit (LEO) satellite and debris orbit predictions is vitally important as space becomes more accessible, especially for satellite owner/operators dedicated to maintaining the safety and sustainability of LEO space. Presently, the primary source of error in orbit predictions stems from uncertainties in the modeling and estimation of thermospheric neutral density. Addressing the need for improved thermospheric observations, SPACEX is partnering with NOAA/NESDIS and SWPC to provide continuous ephemeris, attitude, and housekeeping data from several thousand STARLINK satellites. This work presents the first results of harnessing the SPACEX STARLINK constellation as a signal of opportunity for atmospheric specification and forecasting. By monitoring the dissipation of orbital energy with GNSS measurements, this study presents orbit-effective thermospheric neutral density observations for two STARLINK v1.0 satellites, utilizing them as a case study to demonstrate the methodology. This effort is enabled by augmenting data from the STARLINK onboard navigation filter with a high-fidelity, physics-based characterization of the nonconservative forces and gas-surface interactions. The resulting orbital densities are then compared to those given by the High Accuracy Satellite Drag Model (HASDM). The research showcases the potential of satellite constellations to provide thermospheric observations with unprecedented spatial coverage and contribute to an accurate specification of the thermospheric environment, ultimately enhancing space situational awareness and improving LEO sustainability.

NOMENCLATURE

Variables

A	=	surface area
c	=	speed of light
C	=	normalized aerodynamic force coefficient
$\mathcal{J}$	=	irradiance
k	=	coefficient of reflection
m	=	mass
$\mathbf{n}$	=	surface normal vector
$\mathcal{P}$	=	duration of orbital period
r	=	spacecraft radius
$\mathbf{r}$	=	spacecraft position vector

*Ph.D. Candidate, david.fitzpatrick@colorado.edu, 3775 Discovery Drive, Boulder, CO 80303.
†Senior Research Associate eric.sutton@colorado.edu, 3775 Discovery Drive, Boulder, CO 80303.
‡Research Associate, marcin.pilinski@lasp.colorado.edu, 3665 Discovery Drive, Boulder, CO 80303.

$\mathcal{R}$	=	ratio
s	=	magnitude of the solar position vector relative to the spacecraft
$\mathbf{s}$	=	solar position vector relative to the spacecraft
t	=	time
α	=	energy accommodation coefficient
β	=	smaller angle between the satellite orbital plane and the satellite solar-ecliptic plane
Λ	=	cosine of the angle between satellite solar pointing vector and surface normal
ν	=	shadow function
ρ	=	neutral mass density
τ	=	time variable of integration
ω	=	angular momentum vector

Subscripts and Superscripts

a	=	aerodynamic force
bus	=	satellite bus
cell	=	solar cell
d	=	diffuse
D	=	drag
L	=	lift
M	=	model
O	=	observed
O/M	=	observed-to-model
$\odot$	=	Sun
$\oplus$	=	Earth
ref	=	cross section normal to atmospheric flow
rel	=	relative to the atmospheric flow
s	=	specular
sc	=	spacecraft
SRP	=	solar radiation pressure
Δt	=	effective
X	=	SPACEX
$\hat{}$	=	unit vector
$\dot{}$	=	first time derivative
$\ddot{}$	=	second time derivative

1. INTRODUCTION

The increase in the accessibility of space in recent years brings to the forefront the challenge of quantifying thermospheric neutral density, a critical element of the Low-Earth Orbit (LEO) environment that prevails as the single largest source of error in the prediction of orbits. Unrealistic uncertainties in thermospheric neutral density have significant operational implications, posing challenges for satellite operators and the broader space industry in terms of collision risk assessment, station-keeping maneuver planning, and space traffic regulatory compliance. For many satellite operators, the unavailability of accurate on-orbit atmospheric density forecasts has also been shown to precipitate harsh financial consequences, as demonstrated by the February 2022 STARLINK loss event, which is thought to have resulted in a significant financial loss. The promise of high-accuracy orbital prediction models is dependent upon being able to derive measurements of the upper atmosphere from widely available data products that scale with the spatial density of man-made objects in LEO.

This work seeks to address this need by advancing the accuracy of "nowcasts" and by producing actionable forecasts of thermospheric conditions through the utilization of information from the decay of satellite orbits. To this end, the

Space Exploration Technologies Corporation (SPACEX) has partnered with NOAA's National Environmental Satellite, Data, and Information Service (NESDIS) and Space Weather Prediction Center (SWPC) offices to provide the authors with continuous satellite ephemeris and housekeeping data from several thousand STARLINK satellites. Unlike the small number of satellite missions carrying the scientific-grade accelerometers capable of producing in-situ measurements of neutral density along a single orbital path, the STARLINK constellation has the distinct advantage of simultaneously covering vast swaths of the globe in the aggregate through its multiple orbital planes and string-of-pearls formations. However, compared to near-instantaneous accelerometer measurements, densities derived from the STARLINK constellation must be averaged over some effective time (i.e., one full orbital period) to mitigate errors associated with the measured orbit ephemeris and satellite force model. Moreover, large uncertainties exist in the drag force model caused by a lack of knowledge of the underlying gas-surface collision physics and, to a lesser extent, the accuracy of a satellite's geometry and pointing.

This study provides the first analysis to recover orbit-effective thermospheric neutral density measurements from the SPACEX STARLINK constellation through the techniques of Energy Dissipation Rate (EDR) accelerometry [e.g., 21, 7]. By continuously monitoring the dissipation of orbital energy with Global Navigation Satellite System (GNSS) measurements, orbit-effective thermospheric density observations have been made for STARLINK v1.0 satellites. This effort is enabled by augmenting data from the STARLINK onboard navigation filter with a high-fidelity, physics-based characterization of the nonconservative forces, including drag and lift forces, as well as solar radiation pressure. The fidelity of the improved force model is evaluated by comparing the densities derived from STARLINK with those given by the High Accuracy Satellite Drag Model (HASDM), which is regarded by the United States Space Force (USSF) as the state-of-the-art in thermospheric density models [18].

Section §2 begins with an overview of the STARLINK spacecraft design, followed by a description of the constructed geometry model, operational modes, and nominal attitude profile sequencing per orbit. Section §3 then continues with an introduction of the applied force model in the context of EDR accelerometry, specifying the considered nonconservative accelerations and gas-surface interaction model (GSIM). Next, Section §4 details a comparison of the recovered thermospheric neutral density measurements to HASDM for two selected STARLINK satellites. Finally, Section §5 provides concluding remarks and proposes extensions of this study to a GSIM comparative analysis, as well as model-constrained and data-assimilative frameworks for an improved understanding of thermospheric dynamics.

2. DATASETS: STARLINK

At the forefront of the recent space renaissance are private companies such as SPACEX, with their vision for a large network of interconnected satellites providing global telecommunication services [e.g., 15]. Currently, the majority of the STARLINK constellation is comprised of Generation 1 (Gen1) satellites, including models v1.0 and v1.5, of which the Federal Communications Commission (FCC) has authorized 4,425 in March 2018 [5]. In November 2022, the FCC also authorized SPACEX to deploy 7,500 Gen2 units, each hosting more powerful phased array antennas that allow for signal transmission directly to cell phones [6]. As of 30 August 2024, SPACEX has launched 6,938 Starlink satellites, of which 6,350 are still in orbit [9]. This work focuses on the v1.0 STARLINK satellites contained within Shell 1 (i.e., $\approx 53^\circ$ inclination, $\approx$550 [km] altitude), with future studies planned to include applications to more shells and newer models.

The STARLINK v1.0 satellite design is particularly unique due to its pivoting solar panel, which has an area more than five times larger than the spacecraft bus. This onboard solar panel is controlled through a motorized hinge design that grants the panel a degree of freedom independent of the spacecraft bus. Managed autonomously via onboard flight software, this mechanism allows the solar panel to pivot according to a constrained attitude profile, designed so that the spacecraft can achieve two primary goals: maximizing power generation while maintaining operational pointing for communications. Using the onboard star trackers to determine the spacecraft attitude, the solar panel angle is adjusted to optimize the cosine power loss between the solar panel and the Sun. Simultaneously, the profile also maintains the boresight (i.e., the axis of maximum antenna gain) of the radio patch antennas in a nadir-facing orientation to maximize data downlink capabilities for STARLINK customers. These constraints produce a system with two primary degrees of freedom during nominal operations: a rotation of the spacecraft bus about the Zenith axis and a pivot of the solar panel about its hinge. When the solar panel is positioned at a 90° angle relative to the spacecraft bus, the spacecraft is referred to as being in a "shark-fin" orientation. Conversely, when the panel and bus are co-planar, the spacecraft is described as being in an "open-book" orientation. These orientations are illustrated by Figure 1.

While somewhat complicating on-orbit operations, this dual-focus attitude profile is necessary to balance efficient power generation with optimal communication performance. From the perspective of this study, however, the large variations in the cross-sectional area of the solar panel relative to the atmosphere present a remarkable opportunity for studying gas-surface interactions, discussed more in Section §3.

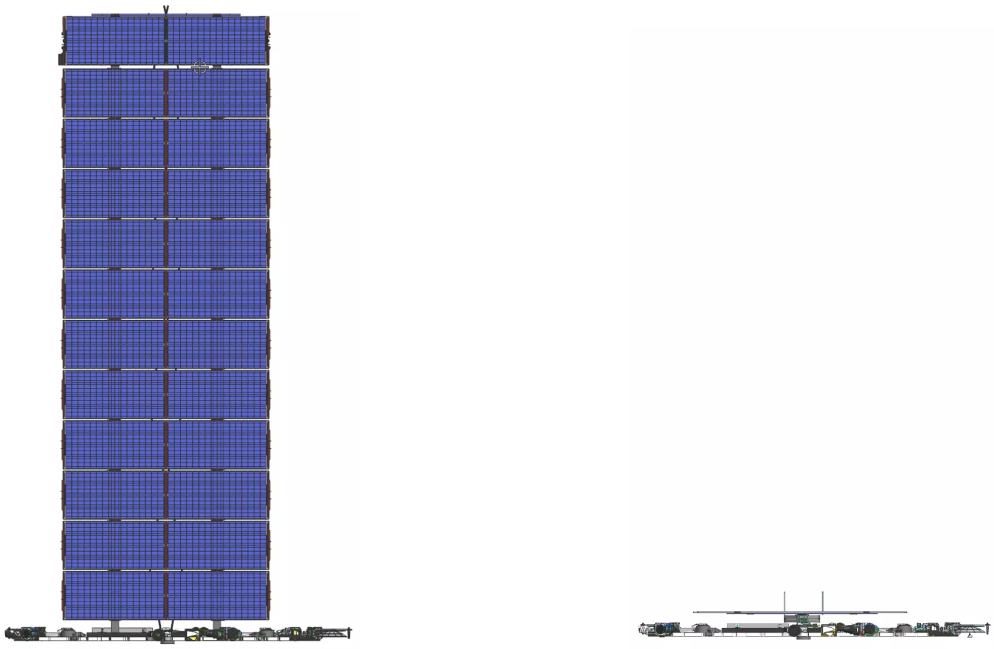

(a) (b)

Fig. 1: Rendering of a STARLINK v1.0 satellite in (a) a shark-fin and (b) an open-book configuration (from www.spacex.com/updates [16]).

In addition to the solar panel, nearly all v1.0 satellites launched since 7 August 2020 have included two sunshade visors to reduce light reflectivity in order to make them less obtrusive to the night sky for astronomical groups [17]. Although these visors are considerably smaller in area than the solar panel, they remain significant for solar radiation pressure and aerodynamic force modeling. The approximate design specifications of the STARLINK v1.0 satellites are detailed in Table 3, while the specific details of the satellite geometry utilized in this study are protected by SPACEX as confidential.

Table 3: Approximate details for the STARLINK v1.0 satellite bus.

Approximate Geometry	
Mass [kg]	260
Spacecraft Bus Nadir/Zenith-Facing Area $\left[\mathrm{m}^2\right]$	4
Solar Panel Area $\left[\mathrm{m}^2\right]$	20
Combined Visor Area $\left[\mathrm{m}^2\right]$	1

Besides the measurements of the spacecraft geometry, SPACEX has provided the authors with position/velocity/time (PVT) data from the onboard Global Positioning System (GPS) receiver, attitude quaternions for both the spacecraft bus and solar panel orientations, as well as pertinent information from the onboard navigation and control filter. SPACEX has also provided housekeeping telemetry data so that times when the satellites are not in an operational mode which is appropriate to the methods described by Section §3 can be filtered out. Periods characterized by propulsive maneuvers for formation keeping and reconfiguration, such as when a new batch of satellites are raised from their commissioning orbit around 210 [km] to operational altitudes, are excluded to avoid unnecessary complications in force modeling.

3. METHODOLOGY

This study applies the Energy Dissipation Rate (EDR) GNSS accelerometry technique detailed by Sutton et al. (2021) [21] and Fitzpatrick et al. (2024) [7] to recover effective thermospheric neutral density, averaged over a continuous single orbital period, from the STARLINK constellation. The EDR GNSS accelerometry technique infers atmospheric neutral density by isolating the orbital energy dissipation solely due to the aerodynamic force. The aerodynamic acceleration corresponding to this force ($\ddot{\mathbf{r}}_\mathrm{a}$) is comprised of the in-track drag ($\ddot{\mathbf{r}}_\mathrm{D}$) and cross-track lift ($\ddot{\mathbf{r}}_\mathrm{L}$) accelerations and can be given by

$$\ddot{\mathbf{r}}_\mathrm{a} = \ddot{\mathbf{r}}_\mathrm{D} + \ddot{\mathbf{r}}_\mathrm{L} = \underbrace{\left(-\frac{\rho}{2m_\mathrm{sc}} C_\mathrm{D} A_\mathrm{ref} \dot{r}_\mathrm{rel} \dot{\mathbf{r}}_\mathrm{rel}\right)}_{\text{drag}} + \underbrace{\left(-\frac{\rho}{2m_\mathrm{sc}} C_\mathrm{L} A_\mathrm{ref} \dot{r}_\mathrm{rel}^2 \hat{\mathbf{r}}_\mathrm{L}\right)}_{\text{lift}}, \tag{1}$$

where the spacecraft speed relative to the atmospheric flow is approximated under the assumption of no winds as $\dot{r}_\mathrm{rel} = \|\dot{\mathbf{r}}_\mathrm{rel}\| \approx \|\dot{\mathbf{r}} - \omega_\oplus \times \mathbf{r}\|$ and the direction of lift $\hat{\mathbf{r}}_\mathrm{L}$ is determined from the satellite geometry and reflection characteristics of the GSIM. All vectors in this study are assumed to be referenced to an inertial coordinate system. While the orthogonal lift force can often be disregarded in many applications, especially when modeling a satellite as a simple sphere, it should not be overlooked for satellites such as STARLINK with geometries which are more susceptible to appreciable lift effects. This study employs the well-established Diffuse Reflection with Incomplete Accommodation (DRIA) GSIM, modified from Sentman (1961) [13] to include the energy accommodation coefficient α according to Sutton (2009) [19], to model the normalized drag (C_D) and lift (C_L) force coefficients.

The observable of the EDR technique is the evaluation of the change in spacecraft orbital energy resulting from collisions with the neutral particles in the thermosphere. Consequently, unlike instantaneous measurements of thermospheric neutral density derived from satellite-borne accelerometer data, the EDR method yields "effective" neutral density measurements integrated over a continuous segment of the orbit, referred to as an "orbit arc." For this study, all orbit arcs are set to span a full orbital period of duration $\mathcal{P}$, with start and end points determined by a sliding window of length $\mathcal{P}$. All integrals are evaluated numerically using trapezoidal integration available from MATLAB.

This work also utilizes the drag acceleration data from the STARLINK onboard navigation filter ($\ddot{r}_\mathrm{D,X}$), in contrast to the approach of Sutton et al. (2021) [21] and Fitzpatrick et al. (2024) [7], which instead evaluates energy dissipation by subtracting the spacecraft's kinetic and potential energy terms. Use of the filter's drag acceleration data circumvents integration errors associated with the gravitational potential gradient, discussed by Fitzpatrick et al. (2024) [7]. This has been shown to improve the EDR signal-to-noise ratio (SNR) for the STARLINK data product. While the instantaneous acceleration values generated by the onboard navigation filter may lack precision, frequent GPS fixes allow the STARLINK navigation filter to adjust the drag acceleration as a fitting parameter to match the true spacecraft state after each full orbital period. Specifically, the drag coefficient is adjusted against the GOST-2004 background drag model [24, 2], ensuring accurate alignment with the actual spacecraft state. This feedback mechanism results in the drag acceleration being well-constrained when integrated over a full orbit to evaluate the energy dissipation.

Although perturbing forces such as third-body gravitational influences and albedo/infrared radiation pressures are considered to be sufficiently modeled by the onboard navigation filter, the solar radiation pressure (SRP) model used in the filter is inadequate for the purposes of this study given the STARLINK design, assuming a spherical satellite with a static cross-sectional area relative to the solar flux vector. This is addressed first by better approximating the shape of a STARLINK v1.0 satellite as a macromodel of N flat plates, a process described by Sutton et al. (2007) [20]. The filter's SRP model is then replaced by an improved formulation from Luthcke et al. (1997) [8] for the SRP acceleration ($\ddot{\mathbf{r}}_\mathrm{SRP}$), which models the force from absorption as well as both the diffuse and specular reflection of radiation forces and computes the total acceleration as the cumulative sum of the contributions from each individual flat plate i. This expression is given by

$$\ddot{\mathbf{r}}_\mathrm{SRP} = -\sum_{\Lambda_i > 0}^{N} \frac{\nu \mathcal{J}_\odot A_i \Lambda_i}{m_\mathrm{sc} c} \left[\hat{\mathbf{s}} + \underbrace{k_{\mathrm{s},i}\left(2\Lambda_i \hat{\mathbf{n}}_i - \hat{\mathbf{s}}\right)}_{\text{specular}} + \underbrace{\frac{2k_{\mathrm{d},i}}{3}\hat{\mathbf{n}}_i}_{\text{diffuse}}\right], \tag{2}$$

where $\Lambda_i = \hat{\mathbf{n}}_i \cdot \hat{\mathbf{s}} > 0$ indicates panel illumination; the shadow function ν (i.e., the proportion of unobscured sunlight) is derived from the Spherical Earth Conical Model [10]; the solar radiation constant at 1 [AU] is given as $\mathcal{J}_\odot = 1353 \left[\mathrm{W \cdot m^{-2}}\right]$ [23]; the speed of light is given as $c = 2.99792458 \times 10^8 \left[\mathrm{m \cdot s^{-1}}\right]$; and the coefficients of specular and diffuse reflection are set to $\{k_\mathrm{s}, k_\mathrm{d}\} = \{0.2, 0.4\}$ for the flat plates corresponding to the satellite chassis as well as the face of the solar panel without solar cells and $\{k_\mathrm{s}, k_\mathrm{d}\} = \{0.05, 0.3\}$ for the face of the solar panel with solar cells. The real-time position of the Sun is approximated using formulas according to *The Astronomical Almanac for the Year 1996* (1995) [22], which cites accuracies to within 0.01° geographic latitude and 0.025° geographic longitude between years 1950 and 2050.

The EDR technique isolates the contributions of aerodynamic interactions to the orbital energy dissipation by subtracting external forces with relevant amplitudes from the aerodynamic force. For this reason, the improved SRP force model is incorporated by adding the SpaceX SRP ($\ddot{\mathbf{r}}_{\mathrm{SRP,X}}$) and drag accelerations calculated by the navigation filter and then subtracting the modeled SRP acceleration $\ddot{\mathbf{r}}_{\mathrm{SRP}}$ detailed by Equation 2. The EDR-observed effective density $\rho^{\mathrm{O}}_{\Delta t}$ for an orbit of length $\Delta t = \mathcal{P}$ beginning at time t can then be found as

$$\rho^{\mathrm{O}}_{\Delta t} = \int_t^{t+\mathcal{P}} \frac{\left(-\ddot{r}_{\mathrm{D,X}}\hat{\mathbf{r}}_{\mathrm{rel}} + \ddot{\mathbf{r}}_{\mathrm{SRP,X}} - \ddot{\mathbf{r}}_{\mathrm{SRP}}\right) \cdot \dot{\mathbf{r}}}{\left(\ddot{\mathbf{r}}_{\mathrm{a}}/\rho\right) \cdot \dot{\mathbf{r}}} \mathrm{d}\tau, \tag{3}$$

where the numerator before integration represents the energy dissipation rate due to the neutral atmosphere and the term $\ddot{\mathbf{r}}_{\mathrm{a}}/\rho$ denotes the evaluation of Equation 1 without the neutral density term ρ. Likewise, the model effective density ($\rho^{\mathrm{M}}_{\Delta t}$) can be found as

$$\rho^{\mathrm{M}}_{\Delta t} = \int_t^{t+\mathcal{P}} \frac{\ddot{\mathbf{r}}_{\mathrm{a}}\left(\rho^{\mathrm{M}}\right) \cdot \dot{\mathbf{r}}}{\left(\ddot{\mathbf{r}}_{\mathrm{a}}/\rho\right) \cdot \dot{\mathbf{r}}} \mathrm{d}\tau, \tag{4}$$

where the term $\ddot{\mathbf{r}}_{\mathrm{a}}\left(\rho^{\mathrm{M}}\right)$ denotes the evaluation of Equation 1 with the instantaneous neutral density term $\rho = \rho^{\mathrm{M}}$ set according to some model or alternative data source (i.e., HASDM [18], NRLMSISE-00 [11], GRACE-FO [14], etc.). This study quantifies the agreement between the EDR-derived observed effective densities and the model output by dividing Equation 3 by Equation 4 to evaluate the observed-to-model ratio ($\mathcal{R}_{\mathrm{O/M}}$) as

$$\mathcal{R}_{\mathrm{O/M}} = \frac{\rho^{\mathrm{O}}_{\Delta t}}{\rho^{\mathrm{M}}_{\Delta t}} = \int_t^{t+\mathcal{P}} \frac{\left(-\ddot{r}_{\mathrm{D,X}}\hat{\mathbf{r}}_{\mathrm{rel}} + \ddot{\mathbf{r}}_{\mathrm{SRP,X}} - \ddot{\mathbf{r}}_{\mathrm{SRP}}\right) \cdot \dot{\mathbf{r}}}{\ddot{\mathbf{r}}_{\mathrm{a}}\left(\rho^{\mathrm{M}}\right) \cdot \dot{\mathbf{r}}} \mathrm{d}\tau. \tag{5}$$

4. RESULTS

Fig. 2 showcases the recovered orbit-average effective thermospheric neutral density measurements according to the EDR method (i.e., $\rho^{\mathrm{O}}_{\Delta t}$ of Equation 3) and HASDM (i.e., $\rho^{\mathrm{M}}_{\Delta t}$ of Equation 4) for Starlink satellites 1008 (top panel) and 2000 (second panel). The observed-to-model ratios (i.e., $\mathcal{R}_{\mathrm{O/M}}$ of Equation 5) are given in the third panel. These satellites are both of the v1.0 design and are located within Shell 1 at an altitude of approximately 550 [km]. The time series covers the period from 1 June 2022 to 1 May 2023, with a few minor data gaps, most notably from the evening of 20 March to 29 March 2023. With the force model specified by DRIA with $\alpha = 0.93$, the EDR-derived density measurements from both spacecraft exhibit trends similar to the estimations by HASDM. This is encouraging given that HASDM is dynamically calibrated against real-time satellite drag observations from its calibration objects, making it the closest approximation to a truth value available. The bottom panel of Fig. 2 details the geomagnetic $\mathrm{a_p}$ index and solar $\mathrm{F_{10.7}}$ index during this period, highlighting periods of enhanced thermospheric activity due to the coupling of the thermosphere with solar processes. The top three panels demonstrate that the EDR-observed effective densities agree with those derived from HASDM to within a factor of the set $[0.5, 1.5]$. Excluding a few outliers, the majority of the ratios are clustered near unity. The consistency of the EDR and HASDM trends, even during periods of enhanced density—such as during the ramping up of the solar cycle around February 2023 and the geomagnetic storms on 27

February 2023 and 23 April 2023—demonstrates the reliability of the EDR method. The EDR-observed and model-based measurements also both show an increasing trend in neutral density over the period of study, aligning with the increase in solar activity as the solar maximum approaches. Additionally, the two satellites exhibit similar trends to each other, despite differences in their design; STARLINK-1008 lacks visors, whereas STARLINK-2000 is equipped with visors. Given that the visors make up a 0 to ≈5% change in the reference area depending on orientation, the similarity in the data-to-model agreement between satellite designs further validates the robustness of the satellite macromodel and the EDR method across varying geometry specifications.

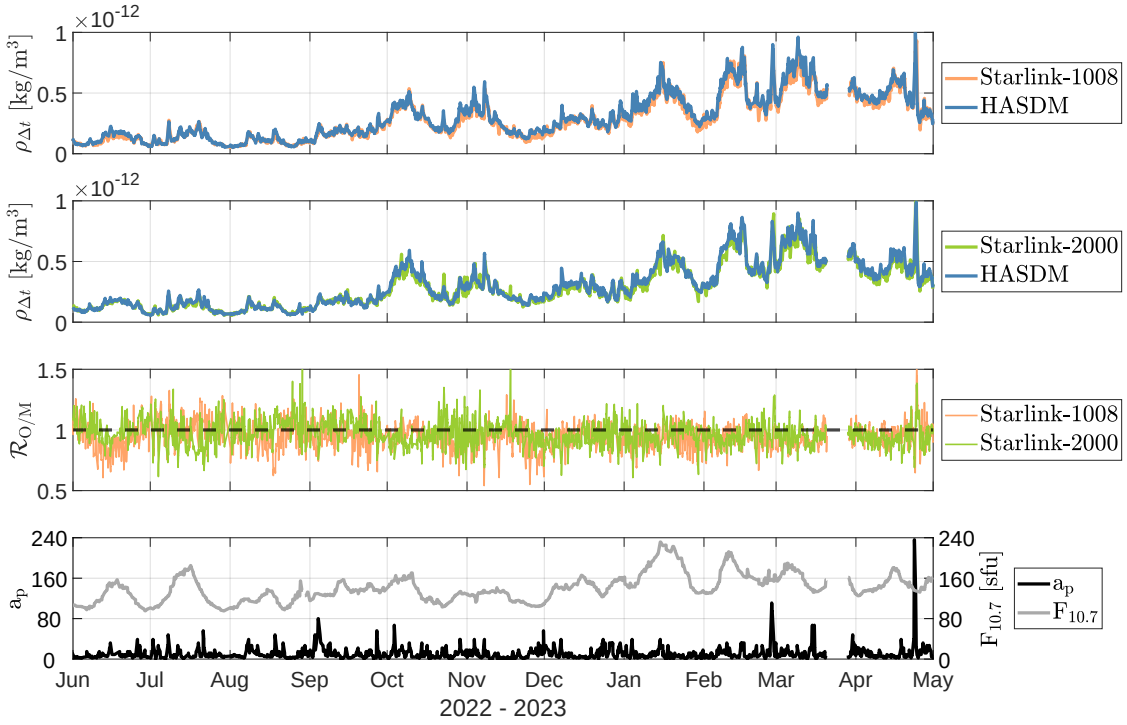

Fig. 2: Time series of the recovered orbit-average effective thermospheric neutral density measurements according to the EDR method (i.e., $\rho^{O}_{\Delta t}$ of Equation 3) and HASDM (i.e., $\rho^{M}_{\Delta t}$ of Equation 4) for STARLINK-1008 and STARLINK-2000, as well as the observed-to-model ratio (i.e., $\mathcal{R}_{O/M}$ of Equation 5) with respect to HASDM, alongside a_p and $F_{10.7}$ indices. The EDR force model is specified by DRIA with $\alpha = 0.93$.

The degree of agreement between the EDR-observed and HASDM-based densities is a function of the fidelity of the force model used to capture the energy dissipation of the satellite, as discussed in Section §3. Although there are numerous ways to tune the force model, this study has found that, given the on-orbit operations and unique shape of the STARLINK satellites, the force model is most sensitive to the GSIM describing the aerodynamic force coefficients. This sensitivity is greater compared to adjustments in other parameters, such as those within the SRP force model. Future work will study the sensitivity of the observed-to-model ratios with respect to HASDM to the description of the gas-surface interactions captured by the parameterization of the GSIM.

5. CONCLUSION AND FUTURE WORK

Enhancing the accuracy of LEO satellite and debris orbit predictions is vitally important as space becomes more accessible, especially for satellite owner/operators dedicated to maintaining the safety and sustainability of LEO space. Presently, the primary source of error in orbit predictions stems from uncertainties in the modeling and estimation of thermospheric neutral density. To address the need of better characterizing the state of the thermosphere, SPACEX

has provided the authors with continuous satellite ephemeris and housekeeping data from several thousand STARLINK satellites. This study takes the first step towards analyzing this rich dataset by applying the Energy Dissipation Rate (EDR) GNSS accelerometry technique to recover orbit-effective neutral density observations for two STARLINK v1.0 satellites. By augmenting data from the STARLINK onboard navigation filter with a high-fidelity, physics-based force model, the EDR-derived densities are compared to the High Accuracy Satellite Drag Model (HASDM). The findings indicate that the applied force model performs well in most instances, demonstrating the reliability and precision of this approach.

Future research will concentrate on several pivotal areas: expanding comparisons to HASDM from single satellite instances to all Gen1 satellites available from the SPACEX data product, enabling the analysis of various local time planes and altitude regions. Additionally, the force model will be refined through a comparative analysis of the employed GSIM. This will involve comparing DRIA against the fundamental approximation of $\{C_\mathrm{D}, C_\mathrm{L}\} = \{2.2, 0\}$ from Cook (1965) [4], evaluating various parameterizations of the Cercignani-Lampis-Lord (CLL) model [3], and assessing hybrid models. One hybrid model will combine DRIA and CLL, while another will be fitted against extrapolated laboratory-derived data based on incident angle and material composition from experiments detailed by Bernstein (2022) [1, 12]. Moreover, the comparisons of the inferred densities will be made against the force model constrained through least-squares minimization Kalman filter techniques to HASDM and/or accelerometer-derived observations from the Gravity Recovery and Climate Experiment Follow-On (GRACE-FO) mission [14]. Once the force model is better understood, this study can also be expanded to develop a data-assimilative framework which ingests the EDR-derived STARLINK densities into a physics-based, operational prediction model such as NOAA/Space Weather Prediction Center's Whole Atmosphere Model (WAM). Data-assimilative techniques such as these represent the future of orbit prediction, enabling more accurate and actionable forecasts of thermospheric conditions. With the potential to integrate additional data sources—further enhancing the coverage and resolution—harnessing commercial satellite datasets will have a profoundly positive impact on space situational and domain awareness.

Utilizing data from the STARLINK constellation marks the first step in a substantial advancement in space weather research. The collaboration with SPACEX represents a significant opportunity for advancing the understanding of the thermosphere, as well as for highlighting the commitment SPACEX has to space sustainability and data sharing. This partnership seeks to benefit satellite operators by contributing to the broader goal of maintaining a sustainable space environment and ensuring the sustainable operation of satellites in this increasingly congested region.

6. ACKNOWLEDGMENTS

The authors gratefully acknowledge David Goldstein and Javier Roa Vicens, of SPACEX, for their invaluable help in obtaining and interpreting raw data from the STARLINK constellation. DJF and EKS were supported in this work by the NOAA/NESDIS Joint Ventures program under award #NA21OAR4310383.

REFERENCES

[1] V. E. Bernstein. *Evaluating Satellite Drag Coefficient Modeling Assumptions in Helium-Rich Space Environments*. PhD thesis, University of Colorado, Boulder, Department of Aerospace and Engineering, January 2022.

[2] Paul Cefola, I. I. Volkov, and V. V. Suevalov. Description of the Russian Upper Atmosphere Density Model GOST-2004. In *37th COSPAR Scientific Assembly*, volume 37, page 476, January 2008.

[3] C. Cercignani and M. Lampis. Kinetic models for gas-surface interactions. *Transport Theory and Statistical Physics*, 1(2):101–114, 1971.

[4] G.E. Cook. Satellite drag coefficients. *Planetary and Space Science*, 13(10):929–946, 1965.

[5] FCC. Space exploration holdings, llc, application for approval for orbital deployment and operating authority for the spacex ngso satellite system, March 2018. Federal Communications Commission Record Citation: 33 FCC Rcd 3391 (4).

[6] FCC. Space exploration holdings, llc request for orbital deployment and operating authority for the spacex gen2 ngso satellite system, November 2022. Federal Communications Commission Record Citation: 37 FCC Rcd 14882 (16).

[7] D. Fitzpatrick, M. Pilinski, R. Bishop, and S. Palo. Applying energy dissipation rate gnss accelerometry to a non-circular orbiting satellite. *Earth and Space Science*, 2024. Manuscript under review.

[8] S. B. Luthcke, J. A. Marshall, S. C. Rowton, K. E. Rachlin, C. M. Cox, and R. G. Williamson. Enhanced radiative force modeling of the tracking and data relay satellites. *The Journal of the Astronautical Sciences*, 45:349–370, 9 1997.

[9] Jonathan McDowell. Jonathan's space pages - starlink statistics. available from vendor site, 2024.

[10] Oliver Montenbruck and Eberhard Gill. *Introductory Astrodynamics*, pages 77–82. Springer Berlin Heidelberg, 2000.

[11] J. M. Picone, A. E. Hedin, D. P. Drob, and A. C. Aikin. Nrlmsise-00 empirical model of the atmosphere: Statistical comparisons and scientific issues. *Journal of Geophysical Research: Space Physics*, 107:SIA 15–1–SIA 15–16, 12 2002.

[12] Marcin Pilinski. *Dynamic Gas-Surface Interaction Modeling for Satellite Aerodynamic Computations*. PhD thesis, University of Colorado, Boulder, 01 2011.

[13] L.H. Sentman. Free molecule flow theory and its application to the determination of aerodynamic forces. pages 265–409. Lockheed Missile and Space Co., TR LMSC-448514, 1961.

[14] Siemes, Christian, Borries, Claudia, Bruinsma, Sean, Fernandez-Gomez, Isabel, Hładczuk, Natalia, den IJssel, Josevan, Kodikara, Timothy, Vielberg, Kristin, and Visser, Pieter. New thermosphere neutral mass density and crosswind datasets from champ, grace, and grace-fo. *J. Space Weather Space Clim.*, 13:16, 2023.

[15] SpaceX. Starlink.com. available from vendor site, 2024. Accessed 16 July 2024.

[16] SpaceX. Starlink.com. available from vendor site, 2024. Accessed 16 July 2024.

[17] SpaceX. Starlink.com. available from vendor site, 8 2024. Accessed 7 May 2024.

[18] Mark F. Storz, Bruce R. Bowman, Major James I. Branson, Stephen J. Casali, and W. Kent Tobiska. High accuracy satellite drag model (hasdm). *Advances in Space Research*, 36(12):2497–2505, 2005. Space Weather.

[19] Eric K. Sutton. Normalized force coefficients for satellites with elongated shapes. *Journal of Spacecraft and Rockets*, 46(1):112–116, 2009.

[20] Eric K. Sutton, R. Steven Nerem, and Jeffrey M. Forbes. Density and winds in the thermosphere deduced from accelerometer data. *Journal of Spacecraft and Rockets*, 44(6):1210–1219, 2007.

[21] Eric K. Sutton, Jeffrey P. Thayer, Marcin D. Pilinski, Shaylah M. Mutschler, Thomas E. Berger, Vu Nguyen, and Dallas Masters. Toward accurate physics-based specifications of neutral density using gnss-enabled small satellites. *Space Weather*, 19(6):e2021SW002736, 2021. e2021SW002736 2021SW002736.

[22] U.S. Government Printing Office. *The Astronomical Almanac for the Year 1996*. U.S. Government Printing Office and Her Majesty's Stationery Office, Washington, D.C. and London, 1996.

[23] David A. Vallado. *Fundamentals of Astrodynamics and Applications*. Microcosm Press, 2013.

[24] I.I. Volkov. Earth's upper atmosphere density model for ballistic support of the flight of artificial earth satellites gost r 25645.166-2004. *Publishing House of the Standards, Moscow*, 2004.